ABUAD Journal of Engineering and Applied Sciences (AJEAS)

ISSN: 2992-5584

Volume 2, Issue 2, 56-65

Solution of Radiative Casson Hybrid Nanofluid Flow in a Permeable Rotating Cone with Nanolayer and Mixed Convection

Soluade Joseph AROLOYE*, Bolaji David AKINPELU

Department of Mathematics, Faculty of Science, University of Lagos, Akoka Yaba, Lagos, Nigeria

saroloye@unilag.edu.ng, akinpelumi.bolaji@gmail.com

*Correspondence: saroloye@unilag.edu.ng; Tel.: +2348073547811

Date Submitted: 01/11/2024
Date Accepted: 16/12/2024
Date Published: 31/12/2024

Abstract: *The research investigates the MHD Casson hybrid nanofluid in the presence of thermal radiation, nanolayers, and mixed convection inside a porous, permeable rotating cone. A slip boundary condition was applied for the problem. The governing flow model describing the problem captures Darcy-Forchheimer, mixed convection, thermal radiation, and dissipation. The coupled PDEs representing flow are obtained and transformed to ODEs via similar variables. The obtained ODEs are solved numerically by the shooting method together with the order six Runge Kutta method. MAPLE mathematical software is used to code and simulate the problem. The effects of embedded flow parameters (tangential and azimuthal velocities, thermal field, Nusselt number, and skin friction coefficient) are presented graphically and in tabular form and discussed in details. The results reveal that higher interfacial nanolayer parameter increases the thermal field. The magnitude of heat transfer rate boosts via greater fluid material and thermal radiation values, while it diminishes through the Prandtl number and Eckert number.*

Keywords: Interfacial layer, viscous dissipation, thermal radiation, Darcy-Forchheimer, Runge Kutta.

1. INTRODUCTION

Hybrid nanofluids exhibit higher thermal performance than conventional nanofluids. Due to improved thermal features of hybrid nanomaterials, these materials can be utilized in laboratory, industrial and engineering devices to enhance their efficiency. Heat transfer enrichment in water-based Al_2O_3 and Al_2O_3–Cu hybrid nanomaterial flow by horizontal circular tube is reported by Moghadassi *et al*. [1]. Hybrid nano fluids are novel fluids that can be formed by submerging different kind of solid tiny particles of metallic elements, carbides, oxides, or carbon nanotubes in base fluids. Hybrid nanofluids observe higher thermal features as compared to nanofluids and are beneficial in industrial and engineering devices. Some applications of hybrid nanomaterials include electronic cooling, car radiators coolant, thermal management in electronics, solar thermal systems, oil and gas industry, heat exchanger, and nuclear plant. Afrand *et al*. [2] investigated the variation in viscosity of SiO_2-MWCNTs/SAE40 hybrid nanofluid versus concentration and temperature of nanoparticles. Mehryan *et al*. [3] re-examined natural convective flow of water-based hybrid nano liquid flow in a cavity having porous walls. Huminic and Huminic [4] theoretically and experimentally investigated thermal enhancement in laminar and turbulent flows of hybrid nanofluids at different concentration and temperature of nanoparticles. Hussan *et al*. [5] investigate behaviour of the hybrid nanomaterial (Ag-CuO) flow in a rotating cone. Xu [6] analysed modelling and analysis of mixed convection flow of hybrid nanomaterial comparing different solid tiny particles between pair of rotating disks. Shatnawi *et al*. [7] examined the influences of various forces on Casson hybrid nano liquid flow with stagnation point. Hussain *et al*. [8] investigated the numerical assessment of hybrid nano liquid flow in a rotating cone considering the effects of intermolecular forces.

Abbas *et al*. [9] investigated numerical assessment for hybrid nanofluid flow by curved stretched sheet in the presence of permeability and slip mechanisms is reported by Heat transfer performance in radiative hybrid nanofluid comparing SWCT/MWCNT is examined by Hussain, *et al*. [10]. Alam *et al*. [11], Arshad *et al*. [12] and Arshad *et al*. [13] carried out various theoretical and experimental investigations on concerning hybrid nanofluid flows over a linear, rotating and stretching geometries problems.

Leong *et al*. [14] and Qureshi *et al*. [15] found that thermal conductivity of nanofluids can be determine effectively using Interfacial nanolayer which has potential usages in liposomes and cell membranes, double layered hydroxide flakes, coolants, and health-testing kits. Rao *et al*. [16] examined thermal conductivity through interfacial layer in melted salt-based nanomaterials. Mohanty *et al*. [17] applied revised Fourier and Fick's law to examine the

https://doi.org/10.53982/ajeas.2024.0202.09-j

features of convective hybrid nanomaterial flow with Darcy-Forchheimer and interfacial nanolayer. Yu and Choi [18] applied a revised Maxwell model with interfacial nanolayer to improve the thermal performance of carrier nano liquids. Fan and Zhong [19] elaborated the impact of influential variables on interfacial layer thickness of water-based hybrid nanofluid. Xie *et al*. [20] examine the role of interfacial nanolayer in enhancement of thermal conductivity of fluid mixture containing nano-sized particles.

Alfven [21] was the first who familiarized the notion of MHD in fluid flows. Kumar and Sivaraj [22] examined the impotence and usefulness of variable viscosity in viscoelastic MHD fluid flow by a moving upright cone and stretched sheet Ashwinkumar *et al*. [23] examined the behaviour of reactive hybrid nanofluid flow caused by flat plate and vertical cone taking radiation effects. Mabood *et al*. [24] applied analytical approach to solve simultaneous effects of binary reaction and MHD near stagnation point flow. Influence of mixed convection and permeably in MHD flow of non-Newtonian fluid by exponentially stretched surface with chemical reaction is examined by Arshad *et al*. [25]. Akhter *et al*. [26] investigated features of MHD hybrid nanofluid in a moderated heated porous cavity with entropy analysis. Physical aspects of convective and zero mass flux restrictions on rotational MHD flow of Prandtl nanofluid with chemical reaction and slip effects is communicated by Sajid *et al*. [27]. Influence of gyrotactic microorganisms in MHD flow of Ellis nanofluid in a rotating permeable cone is reported by Ahmed *et al*. [28]. Abbas *et al*. [29] explored magnetized flow of micro polar nano liquid considering the features of velocity slip, variable thermal conductivity, heat generation and thermal radiation. Arshad *et al*. [30] explored the characteristics of MHD viscoelastic non-compressible nano liquid fluid flow in the presence of absorbent shrinking/extending surface.

The Darcy–Forchheimer (DF) model capture the nature of flow in which the flow rate throughout the stream by means of pressure gradient, viscosity and permeability of surface. Haider *et al*. [31] explored the characteristics of steady DF flow of hybrid nanofluid in a rotating permeable frame with radiation Flows over the surfaces with porous medium has vital usages in mechanical, technical and industrial fields such as atomic waste archive, catalytic converters, improved oil recuperation, gas turbine, grain stockpiling energy production, and atherosclerosis. Khan *et al*. [32] investigated thermal enhancement in radiative DF flow together with chemical reaction and heat generation. Caucao and Discacciati [33] expanded weak and strong formulation for Brinkman–Forchheimer in two-dimensional fluid flow. Abbas *et al*. [34] explored the heat transport in radiated DF flow over permeable sphere. Maatoug *et al*. [35] applied experimental procedure to study behaviour of squeezed DF flow of Jeffrey nanomaterial with heat generation and activation energy. Abbas *et al*. [36] examined the features of DF resistance in radiated nanomaterial flow with stretched cylinder and chemical reaction.

Based on the above aforementioned in the literature, there is no research work on that jointly address DF flow model with cluster interfacial layer and hybrid nanofluid saturated with tiny particles in the presence of thermal radiations over a rotational cone. Our aim is to model and analyze Casson hybrid nanofluid flow saturated with nanoparticles inside a rotation cone in the presence of cluster interfacial layer, slip boundary conditions, heat generation, thermal radiation and viscous dissipation. The obtained models in the form of highly couple non-linear Partial differential equations are transform to system of ordinary differential equations. The resulting ODEs is simulated numerically with aid of MAPLE mathematical software.

2. MATERIAL AND METHODS

2.1 Problem Formulation

We consider three dimensional, Laminar, steady, Darcy Forchheimer flow of Casson nanofluid confined in a rotating cone saturated with nanoparticle is considered in the presence of thermal radiation, viscous dissipation, permeability and heat generation Thermal radiation and dissipation effects are incorporated into energy transport equations. The velocity slip and interfacial nanolayer are also developed. The flow governing Equations (1), (2), (3), (4) and (5) are acquired through boundary layer suppositions as investigated by Ali [37] and Kiran *et al*. [38].

$$(xw)_z + (xu)_x = 0 \tag{1}$$

$$\rho_{hnf}\left(uu_x + wuz - \frac{v^2}{x}\right) = \mu_{hnf}\left(\frac{1}{\beta}+1\right)\frac{\partial^2 u}{\partial z^2} + \rho_{hnf} g\beta_T (T - T_\infty)\cos\alpha \; - \frac{\mu_{hnf}}{K^*}u - \rho Feu^2 \tag{2}$$

$$\rho_{hnf}\left(u\frac{\partial y}{\partial x} + w\frac{\partial v}{\partial z} + \frac{uv}{x}\right) = \mu_{hnf}\left(\frac{1}{\beta}+1\right)v_z^2 - \frac{\mu_{hnf}}{K^*}v - \rho_{hnf} Fev^2 + \frac{Q}{(pC_p)_{hnf}}(T_x + T_z) \tag{3}$$

$$uT_x + wT_z = \frac{k_{hnf}}{(pC_p)_{hnf}}\left(1 + \frac{4^2\sigma^* T_\infty^2 T_\infty}{3k^* k_{hnf}}\right)\frac{\partial^2 T}{\partial z^2} + \frac{\mu_{hnf}}{(pC_p)_{hnf}}\left(1+\frac{1}{\beta}\right)\left(\left(\frac{\partial u}{\partial z}\right)^2 + \left(\frac{\partial v}{\partial z}\right)^2\right) - \frac{1}{(pC_p)_{hnf}}\frac{\partial qr}{\partial y} \tag{4}$$

With

$$\left.\begin{array}{c} u = \frac{2-\sigma_v}{\sigma_v}\lambda_o u_z,\; v = \Omega x\sin\alpha^* + \frac{2-\sigma_v}{\sigma_v}\lambda_o u_z \; at\; y = 0 \\ T = \frac{-\sigma_T+2}{\sigma_T}\left(\frac{2r}{r+1}\right)\frac{\lambda_o}{P_r}\frac{\partial T}{\partial z} + T_w \; at\; w = 0 \\ v = 0,\; T \to T_\infty,\; u \to 0 \; as\; y \to \infty. \end{array}\right\} \tag{5}$$

Following Hassan *et al*. [5] and Ali [37], the thermo-physical characteristics of hybrid nanofluid are mathematically defined as shown in Equations (6) to (15).

$$\rho_{hnf} = \Phi_1\rho_{s1} + \Phi_2\rho_{s2} - (1 - \Phi_1 - \Phi_2)\rho_{bf} \tag{6}$$

$$\mu_{hnf} = \frac{\mu_{bf}}{(1-\Phi_1-\Phi_2)^{2.5}} \tag{7}$$

$$(\rho C_p)_{hnf} = \Phi_1(\rho C_p)(\rho C_p)_{s1} + \Phi_2(\rho C_p)(\rho C_p)_{s2} + (1-\Phi_1-\Phi_2)(\rho C_p)_{bf} \quad (8)$$

$$\frac{k_{hnf}}{k_{bf}} = \frac{(k_{p2}-k_{nlr})\Phi_{s2}k_{nlr}(\lambda_2^2-\lambda_1^2+1)+(k_{p2}+k_{nlr})\lambda_2^2(\Phi_{s2}\lambda_1^2)}{(\lambda_2^2(k_{p2}+k_{nlr})-(k_{p2}-k_{nlr})\Phi_{s2}(\lambda_2^2+\lambda_1^2-1)k_{bf}} \quad (9)$$

$$\frac{k_{mbf}}{k_f} = \frac{(k_{p1}-k_{nlr})\Phi_{p1}k_{nlr}(\lambda_2^2-\lambda_1^2+1)+(k_{p1}+k_{nlr})}{(\lambda_2^2(k_{p1}+k_{nlr})-(k_{p1}-k_{nlr})\Phi_{p1}(\lambda_2^2+\lambda_1^2-1)k_f} \quad (10)$$

Considering,

$$\left.\begin{array}{c} u = \frac{-1}{2}\Omega x \sin\alpha^* f', v = \Omega x \sin\alpha^* g,\ \theta(\eta) = \frac{T-T_\infty}{T_w-T_\infty}, \\ w = \sqrt{\Omega v_o \sin\alpha}\, f(\eta), \\ \eta = \sqrt{\frac{\Omega\sin\alpha^*}{v_o}} Z,\ T_w = T_\infty + \frac{x(T_o-T_\infty)}{l} \end{array}\right\} (11)$$

We get

$$G_1\left(1+\frac{1}{\beta}\right)f''' + \left(\frac{1}{2}f'^2 - 2g.g - ff'' + \frac{1}{2}Frf'^2 - 2\lambda\theta\right) - \varsigma G_1 f'(\eta) = 0 \quad (12)$$

$$G_1\left(1+\frac{1}{\beta}\right)g''(\eta) - (f'g + fg' + Frg^2) - \varsigma g G_1 = 0, \quad (13)$$

$$(1+Rd)\theta'' + G_2G_3Pr\left(\frac{1}{2}f'\theta - f\theta' + G_4\right)PrEc\left(1+\frac{1}{\beta}\right)\left(\frac{1}{4}f''^2 + g'^2\right) = 0 \quad (14)$$

$$\left.\begin{array}{c} f'(\eta) = \gamma_1 f'',\ f(\eta) = 0,\ g = \gamma_1 g' + 1,\ \theta \\ = \gamma_2\theta' + 1\ at\ \eta = 0 \\ f'(\eta)\to 0, g(\eta)\to 0,\ \theta(\eta)\to 0\ as\ \eta\to\infty \end{array}\right\} (15)$$

where G_1, G_2, and G_3 are given as shown in Equation (16):

$$\left.\begin{array}{c} G_1 = ((1-(\Phi_1+\Phi_2))^{2.5} \\ \left(\begin{array}{c}(1-(\Phi_1+\Phi_2))+\\ (\Phi_1)\left(\frac{\rho_{s1}}{\rho_{bf}}\right)\\ +(\Phi_2)\left(\frac{\rho_{s2}}{\rho_{bf}}\right)\end{array}\right)^{-1} \\ G_2 = (1-(\Phi_1+\Phi_2)+(\Phi_1)\left(\frac{\rho_{cps1}}{\rho_{cpbf}}\right) \\ + \\ (\Phi_2)\left(\frac{\rho_{cps2}}{\rho_{cpbf}}\right)), \\ G_3 = (\frac{k_{hnf}}{k_{mbf}}\frac{k_{mbf}}{k_f})^{-1} \end{array}\right\} (16)$$

where

$$\left.\begin{array}{c} Fr = \frac{Cb}{\sqrt{K^*}},\ Fe = F\Omega x\sin\alpha^*,\ \varsigma = \frac{1}{\Omega x\sin\alpha^* K^*}, \\ \lambda = \frac{Gr}{Re^2},\ Re = \frac{L^2\Omega\sin\alpha^*}{v} \\ Gr = \frac{g\beta_T\cos\alpha^*(T_w-T_\infty L^3)}{v^2},\ Pr = \frac{\mu Cp}{k_f}, \\ \gamma_1 = \frac{2-\sigma_v}{\sigma_v}\lambda_o\sqrt{\frac{\Omega\sin\alpha^*}{v}} \\ Ec = \frac{(\Omega x\sin\alpha^*)^2L^2}{C_p(T_w-T_\infty)},\ Rd = \frac{16\sigma T_\infty{}^3}{3K^*K_\infty}, \\ \lambda_2 = \left(\frac{2r}{r+1}\right)\frac{-\sigma_T+2}{\sigma_T}\frac{\lambda_o}{Pr}\sqrt{\frac{\Omega\sin\alpha^*}{v}} \end{array}\right\} (17)$$

2.2 Physical Engineering Quantities

Skin friction coefficient and Nusselt number can be defined as shown in Equations (18) – (20).

$$\left.\begin{array}{c} Cf_x = \frac{2\tau_{xz}}{\rho_f\Omega^2x^2sin^2\alpha},\ Cf_y = \frac{2\tau_{yz}}{\rho_f\Omega^2x^2sin^2\alpha}, \\ Nu_x = \frac{xq_w}{k_f(T_w-T_\infty)}. \end{array}\right\} (18)$$

where

$$\left.\begin{array}{c} \tau_{xz} = \mu_{hnf}\left(1+\frac{1}{\beta}\right)\frac{\partial u}{\partial z}, \\ \tau_{yz} = \mu_{hnf}\left(1+\frac{1}{\beta}\right)\frac{\partial v}{\partial z}, \\ q_w = -\left(k_{hnf} + \frac{16\sigma^*T_\infty{}^3}{3k^*}\right)\frac{\partial T}{\partial z} \end{array}\right\} (19)$$

Finally,

$$\left.\begin{array}{c} Cf_{xz}Re_x{}^{1/2} = -\left(1+\frac{1}{\beta}\right)f''\frac{1}{(1-\phi_1-\phi_2)^{2.5}}, \\ Cf_{yz}Re_x{}^{1/2} = -\left(1+\frac{1}{\beta}\right)g'\frac{1}{(1-\phi_1-\phi_2)^{2.5}} \\ Nu_xRe_x{}^{1/2} = -\frac{k_{hnf}}{k_f}(1+Rd)\theta' \end{array}\right\} (20)$$

2.3 Numerical Solution

The shooting method alongside with six order Runge-Kutta integration scheme, with the help of MAPLE Mathematical software is used to solve the system of highly non-linear differential Equations (12), (13) and (14) subjected to boundary conditions (15) for different moderate values of the flow, heat and mass transfer parameters. The effective Broyden technique is adopted in order to improve the initial guesses and to satisfy the boundary conditions at infinity. Maple software is used to code and simulate the above numerical procedure

3. RESULTS AND DISCUSSION

Table 1 shows results validation for numerical method applied in this paper. In the table, the present results were compared with that of Kiran *et al* [38] and Li *et al*. [39] and there is excellent agreement. This helps validate the results in this paper.

Table 1: Comparison of results for skin friction coefficient when P_r = 7.38

λ	Li *et al*. [39]	Kiran [38]	Present Result
0.0	1.02551	1.03012	1.0301201

λ	Li *et al*. [39]	Kiran [38]	Present Result
1.0	2.20102	1.03011	1.0301101
10.0	8.50421	8.50422	8.5042202

Table 2: Computations result for skin friction coefficient $f'(0)$ and Nusselt number $\theta(0)$

β	λ	Fr	ξ	λ_1	$f'(0)$	$\theta(0)$
1.1	0.6	1.3	0.2	0.6	1.6894	0.2098
1.4					1.5642	0.3476
1.8					1.4098	0.4987
	0.4				0.7843	1.3456
	0.5				0.8764	1.4539
	0.7				1.2876	1.5674
		1.3			1.0758	1.7875
		1.6			1.0568	1.6754
		1.9			1.0468	1.4897
			0.9		0.6537	0.5609
			1.1		0.6100	0.4563
			1.3		0.5893	0.3456
				1.1	0.7784	0.6785
				1.6	0.4954	0.5642
				2.1	0.8906	0.4980

Table 2 is generated to examine the influence of shows the results of physical impacts of $\beta, \lambda, Fr, \varsigma, and\ \gamma_1$ on skin friction coefficient/surface drag forces $\left(Cf_x Re_x^{1/2}\right)$ and Nusselt number/heat transfer rate $\left(Nu_x Re^{1/2}\right)$ through $\beta, \lambda, Fr, \varsigma, and\ \gamma_1$. From Table 2, it is observed that intensity of $Cf_x Re_x^{1/2}$ accelerates for rising $\lambda, Fr, and\ \varsigma$ while a decay is noticed in the case of $\beta\ and\ \gamma_1$ and local heat rate $Nu_x Re^{1/2}$ increases through large value of $\beta\ and\ Rd$ while it diminished through $Ec, Pr, and\ \gamma_2$.

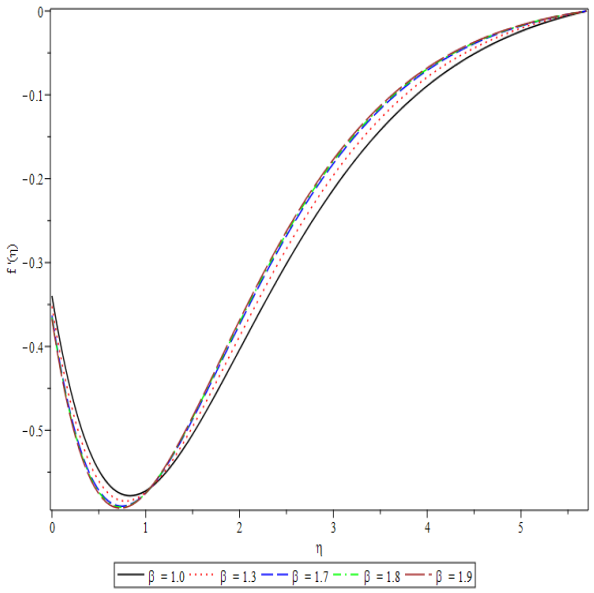

Figure 1: Fluctuation in $f'(\eta)$ versus β

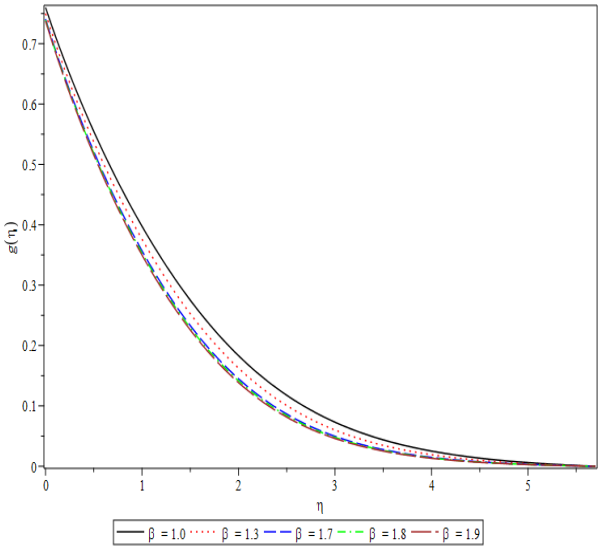

Figure 2: Fluctuation in $g(\eta)$ versus β

Physical impact of fluid material variable (β) on tangential and azimuthal velocities is plotted in Figures 1 and 2. Tangential velocity $f'(\eta)$ increases while azimuthal velocity $g(\eta)$ decays for larger values of β. Since higher β improves the material dynamic velocity, thus yield stress decays and as a result $g(\eta)$ decays but $f'(\eta)$ decreases near the porous plate surface plate, as $\beta \longrightarrow \infty$, $f'(\eta)$ enhances. Figures 3 and 4 are plotted to explain the nature of $f'(\eta)$ and $g(\eta)$ via higher Forchheimer variable (Fr). Apparently, curves of $f'(\eta)$ and $g(\eta)$ show opposite behaviour when Fr takes higher estimations. Physically, greater Fr increases restart resistance to the flow and thus $g(\eta)$ decreases while $f'(\eta)$ accelerates. The effect of permeability of surface on velocities $\left(f'(\eta),\ g(\eta)\right)$ is depicted in Figures 5 and 6. Both $f'(\eta)$ and $g(\eta)$ diminished for larger values of λ. For higher λ laager values, size of holes of porous surface expands and thus more resistance is offered from surface to the fluid. Therefore, $f'(\eta)$ and $g(\eta)$ decreased.

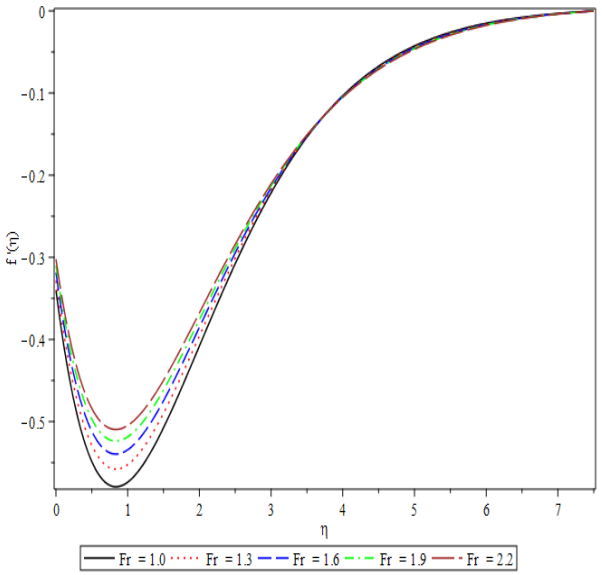

Figure 3: Fluctuation in $f'(\eta)$ versus Fr

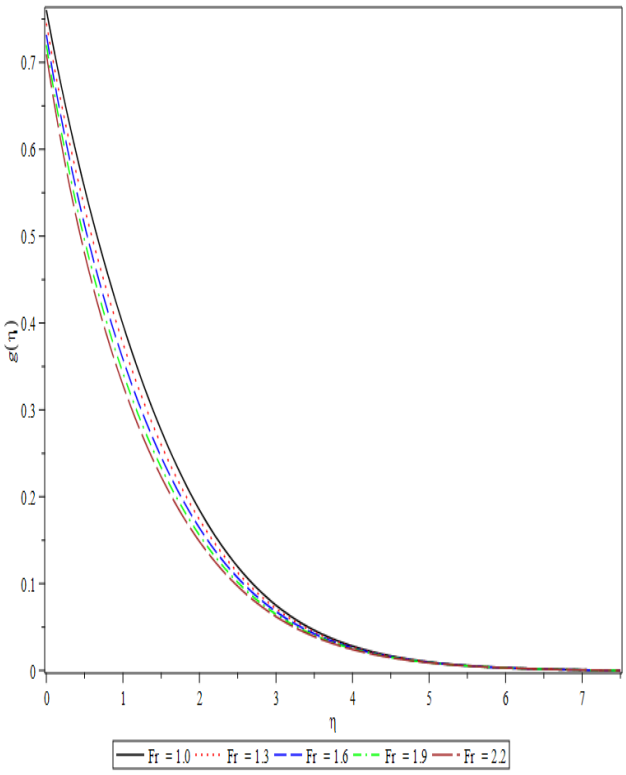

Figure 4: Fluctuation in $g(\eta)$ versus Fr

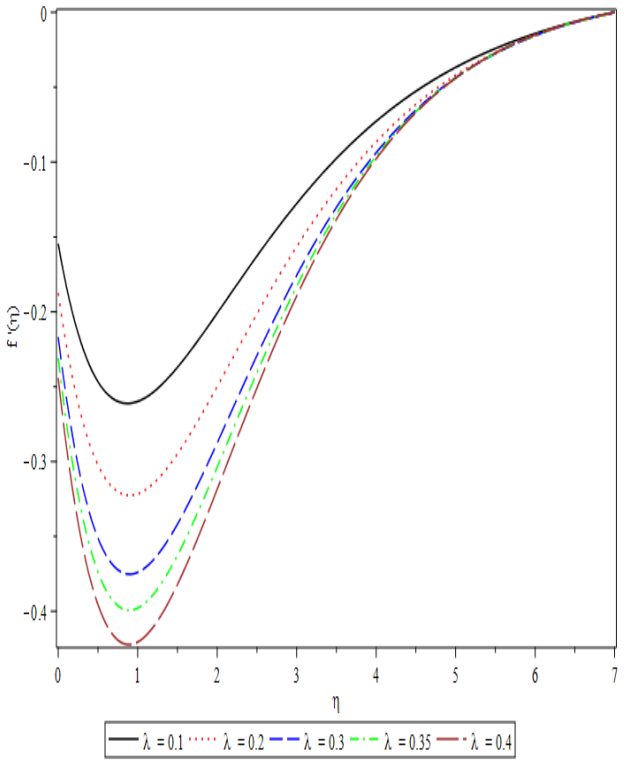

Figure 5: Fluctuation in $f'(\eta)$ versus λ

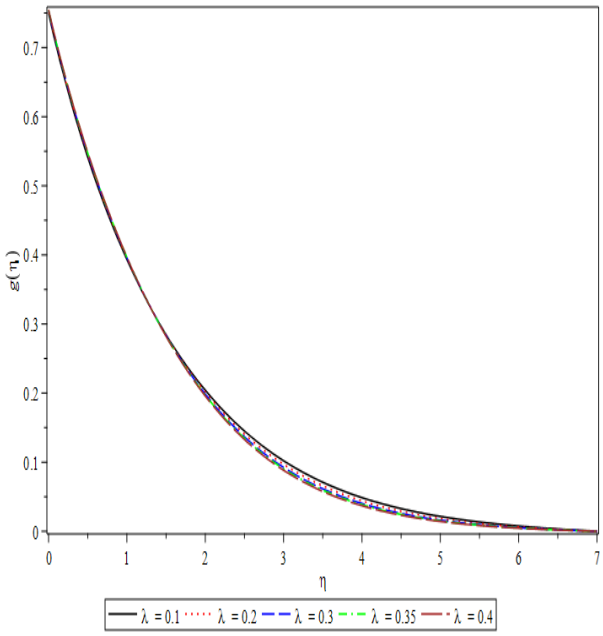

Figure 6: Fluctuation in $g(\eta)$ versus λ

The influence and impact of mixed convection variable on hybrid nanofluid velocities $(f'(\eta),\ g(\eta))$ are depicted in Figures 7 and 8. One can observe that $f'(\eta)$ increases, whereas $g(\eta)$ decreases via rising ς. Figure 9 was plotted to depict the impact of γ_1 on $f'(\eta)$. In fact, γ_1 has direct relationship with wall shear strain. Higher values of γ_1 increases $f'(\eta)$. Characteristics of hybrid nanofluid thermal field($\theta(\eta)$) versus influential variables like Prandtl number (Pr), Eckert number (Ec), nanolayer parameter(λ_1) and radiation variable (Rd) are examined through Figures 10–13. Physical impact of Pr on $\theta(\eta)$ is portrayed in Figure 10. Thermal field decreased as Pr decreases. Since thermal diffusivity reduces versus rising Pr estimations and thus thermal field decays. Figure 11 was plotted to study the influence of Ec on $\theta(\eta)$. Clearly, higher dissipative variable retards the hybrid thermal field. Improvement in Ec increases the process of conversion of kinetic energy into system internal energy. Therefore, curves of $\theta(\eta)$ fall down. Figure 12 was plotted to explore the variation in $\theta(\eta)$ against higher λ_1; here, temperature field expands and the boundary layer width grows with a rise in the λ_1. In Figure 13, variation in thermal field via higher Rd was captured. Here, curves of $\theta(\eta)$ improve via rising values of thermal radiation Rd. Since higher Rd supplies more heat to the system, thus $\theta(\eta)$ increases.

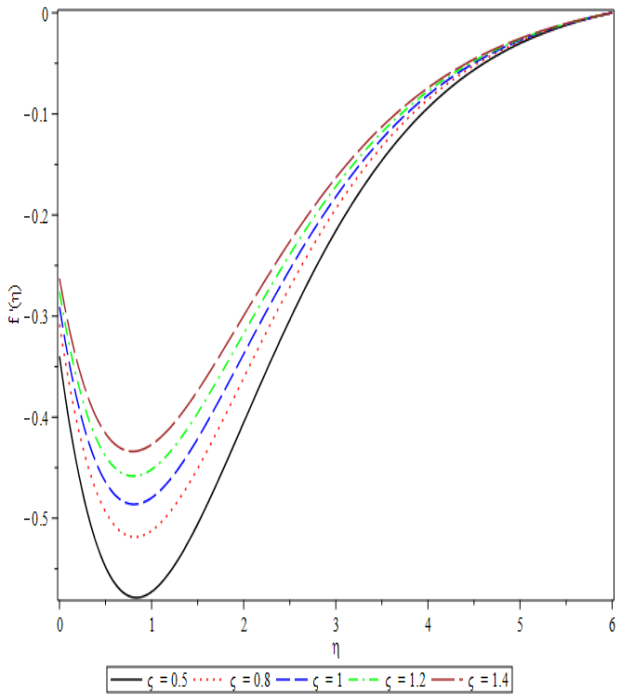

Figure 7: Fluctuation in $f'(\eta)$ versus ς

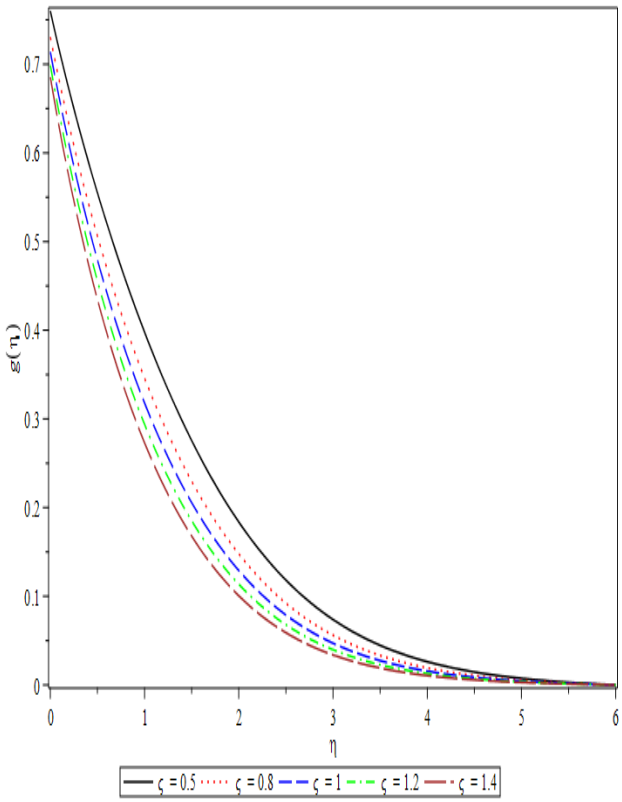

Figure 8: Fluctuation in $g(\eta)$ versus ς

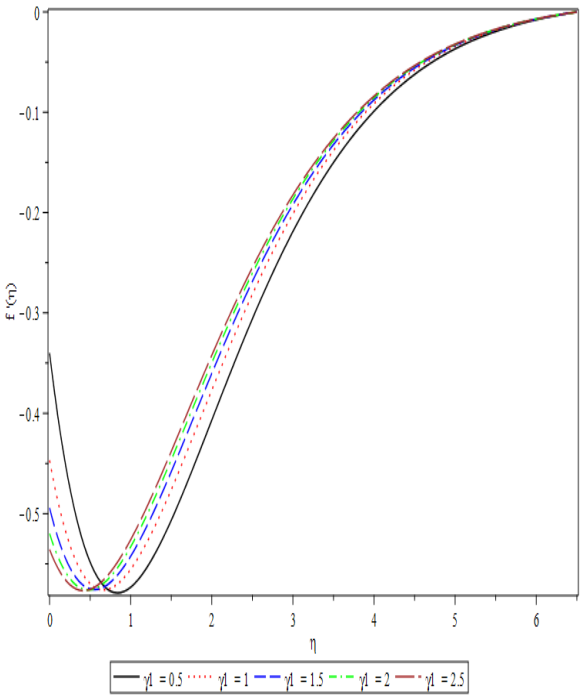

Figure 9: Fluctuation in $f'(\eta)$ versus γ_1

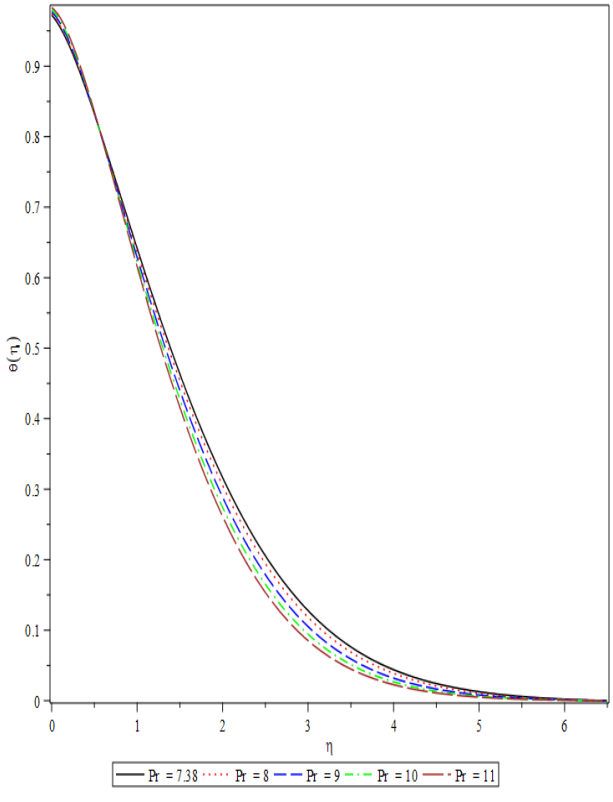

Figure 10: Fluctuation in $\theta(\eta)$ versus Pr

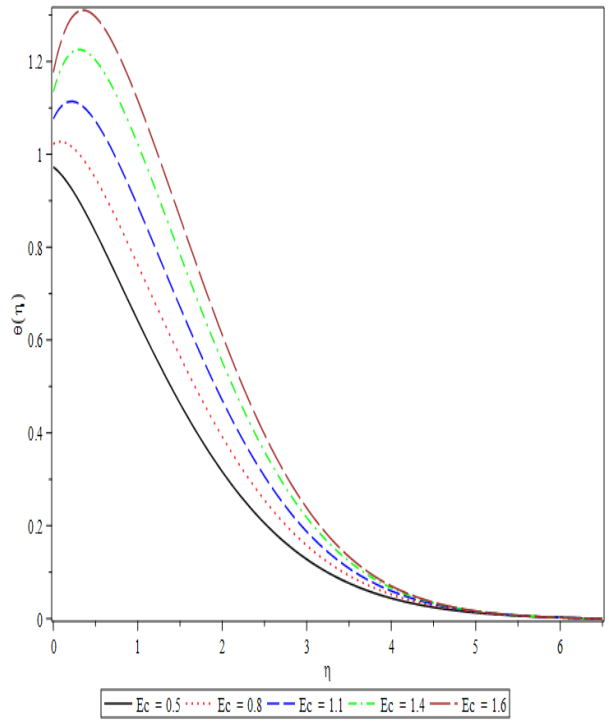

Figure 11: Variation in $\theta(\eta)$ versus Ec

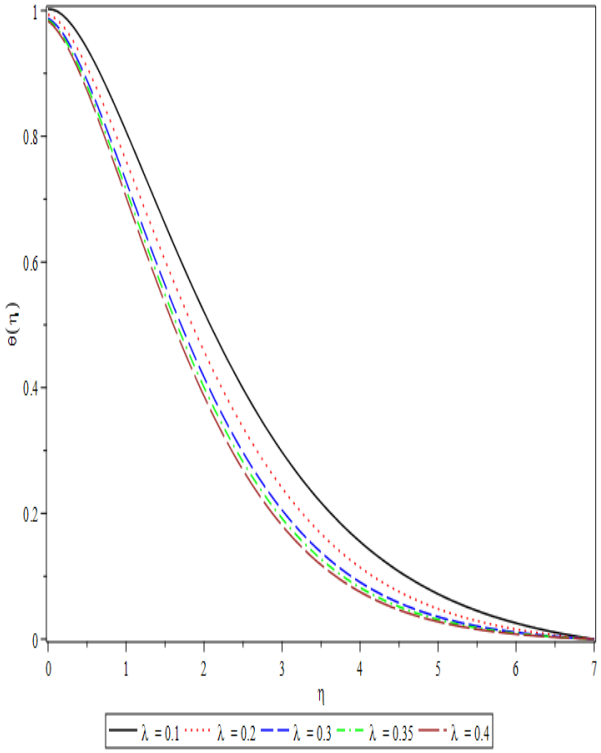

Figure 12: Fluctuation in $\theta(\eta)$ versus λ_1

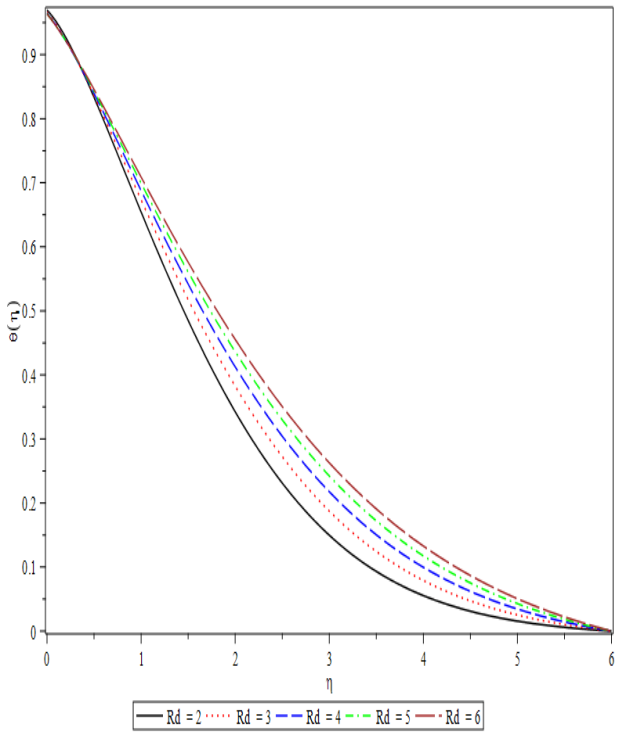

Figure 13: Variation in $\theta(\eta)$ versus Rd

4. CONCLUSION

In this paper, flow behaviour of hybrid Casson nanofluid in a permeable rotating cone with interfacial nanolayer was highlighted. The influences of mixed convection, Darcy resistance, dissipation, and radiation were considered. The dimensionless equations representing the flow were solved numerically via SOR technique in MAPLE. The following list summarizes the key outcomes of this study. Velocities decrease with increasing nanoparticle volume fraction (ϕ2) and Darcy number (λ), while increasing rotation parameter (β), Froude number (Fr), and magnetic field strength (ς) enhance velocities. Thermal field enhancement was observed with increasing Eckert number (Ec), thermal conductivity parameter and nanoparticle volume fractions, whereas Prandtl number reduces thermal field. Skin friction coefficient increases with λ, Fr, and ς, but decreases with β and γ_1.

NOMENCLATURE

(x, z)	Cartesian coordinates
ρ	Fluid density
g	Gravitational force
K^*	Permeability of porous medium
T_o	Characteristic temperature
k	Thermal conductivity
C_p	Specific heat
k^*	Mean absorption coefficient
(Φ_1, Φ_2)	Volume fraction of nanoparticles
(Ω_1, Ω_2)	Angular velocities
λ	Mixed convection parameter
T_∞	Ambient temperature
$(f'(\eta),\ g(\eta))$	Tangential and azimuthal velocities

Rd Radiation parameter
Gr Grashof number
(τ_{xz}, τ_{yz}) Shear stresses
Nu_x Nusselt number

Subscripts

f Fluid
nf Nanofluid
s_1 Volume fraction of zinc spinal ferrite ($Mn-Zn\ Fe_2O_4$).
nlr Thermal conductivity of nanolayer
hnf Hybrid nanoparticles
s_2 Volume fraction of cobalt ferrite ($CoFe_2O_4$)
bf Base fluid
θ Dimensionless temperature
(u, v, w) Velocity components
μ Dynamic viscosity
T Fluid temperature
Fe Inertia coefficient
β Cassion fluid material constant
σ^* Stefan- Boltzmann constant
α^* Inclination angle
Pr Prandtl number
T_w Surface temperature
(λ_1, λ_2) Nanolayer thickness
Fr Inertia parameter
ς Permeability variable
γ_1 Velocity slip parameter
γ_2 Temperature slip parameter
Ec Eckert number
(Cf_x, Cf_y) Skin friction coefficients
q_w Radiative heat flux

REFERENCES

[1] Moghadassi, A., Ghomi, E., and Parvizian, F. (2015). A numerical study of water based Al_2O_3 and Al_2O_3–Cu hybrid nanofluid effect on forced convective heat transfer. *International Journal of Thermal Sciences, 92*, 50–57.

[2] Afrand, M., Najafabadi, K.N. and Akbari, M., (2016). Effects of temperature and solid volume fraction on viscosity of SiO_2-MWCNTs/SAE40 hybrid nanofluid as a coolant and lubricant in heat engines. *Applied Thermal Engineering*, *102*, pp.45-54.

[3] Mehryan, S. A. M., Kashkooli, F. M., Ghalambaz, M., and Chamkha, A. J. (2017). Free convection of hybrid Al_2O_3-Cu water nanofluid in a differentially heated porous cavity. *Advanced Powder Technology*, *28*(9), 2295–2305.

[4] Huminic, G. and Huminic, A. (2018). Heat transfer capability of the hybrid nanofluids for heat transfer applications. *Journal of Molecular Liquids*, *272*, pp.857-870.

[5] Hassan, A., Hussain, A., Arshad, M., Haider, Q., Althobaiti, A., Elagan, S. K., Alqurashi, M.S. and Abdelmohimen, M. A. (2022). Heat transport investigation of hybrid nanofluid (Ag-CuO) porous medium flow: Under magnetic field and Rosseland radiation. *Ain Shams Engineering Journal*, *13*(5), p.101667.

[6] Xu, H. (2019). Modelling unsteady mixed convection of a nanofluid suspended with multiple kinds of nanoparticles between two rotating disks by generalized hybrid model. *International Communications in Heat and Mass Transfer*, *108*, 104275.

[7] Shatnawi, T. A., Abbas, N., and Shatanawi, W. (2022). Comparative study of Casson hybrid nanofluid models with induced magnetic radiative flow over a vertical permeable exponentially stretching sheet. *AIMS Math*, *7*(12), 20545-20564.

[8] Hussain, A., Hassan, A., Arshad, M., Rehman, A., Matoog, R. T., and Abdeljawad, T. (2021). Numerical simulation and thermal enhancement of multi-based nanofluid over an embrittled cone. *Case Studies in Thermal Engineering*, *28*, 101614.

[9] Abbas, N., Rehman, K. U., Shatanawi, W., and Malik, M. Y. (2022). Numerical study of heat transfer in hybrid nanofluid flow over permeable nonlinear stretching curved surface with thermal slip. *International Communications in Heat and Mass Transfer*, *135*, 106107.

[10] Hussain, A., Hassan, A., Al Mdallal, Q., Ahmad, H., Rehman, A., Altanji, M., and Arshad, M. (2021). Heat transport investigation of magneto-hydrodynamics (SWCNT-MWCNT) hybrid nanofluid under the thermal radiation regime. *Case Studies in Thermal Engineering*, *27*, 101244.

[11] Alam, M. M., Arshad, M., Alharbi, F. M., Hassan, A., Haider, Q., Al-Essa, L. A., Eldin, S. M., Saeed, A. M. and Galal, A. M. (2023). Comparative dynamics of mixed convection heat transfer under thermal radiation effect with porous medium flow over dual stretched surface. *Scientific Reports*, *13*(1), p.12827.

[12] Arshad, M., Alharbi, F. M., Hassan, A., Haider, Q., Alhushaybari, A., Eldin, S. M., Ahmad, Z., Al-Essa, L. A. and Galal, A. M. (2023). Effect of inclined magnetic field on radiative heat and mass transfer in chemically reactive hybrid nanofluid flow due to dual stretching. *Scientific Reports*, *13*(1), p.7828.

[13] Arshad, M., Alharbi, F. M., Alhushaybari, A., Eldin, S. M., Ahmad, Z., and Galal, A. M. (2023). Exploration of heat and mass transfer subjected to first order chemical reaction and thermal radiation: Comparative dynamics of nano, hybrid and tri-hybrid particles over dual stretching surface. *International Communications in Heat and Mass Transfer*, *146*, 106916.

[14] Leong, K. C., Yang, C., and Murshed, S. M. S. (2006). A model for the thermal conductivity of nanofluids – the effect of interfacial layer. *Journal of Nanoparticle Research*, *8*(2), 245–254.

[15] Qureshi, M. Z. A., Raza, Q., Ramzan, A., Faisal, M., Ali, B., Shah, N. A., and Weera, W. (2022).

Activation energy performance through magnetized hybrid Fe_3O_4–PP nanofluids flow with impact of the cluster interfacial nanolayer. *Mathematics*, *10*(18), 3277.

[16] Rao, Z., Bai, R., Ye, K., and Zhou, T. (2022). Effects of interfacial layer on thermal conductivity enhancement of solar salt-based nanofluids: Insights from molecular dynamics simulations. *Case Studies in Thermal Engineering*, *35*, 102087.

[17] Mohanty, D., Sethy, N., Mahanta, G., and Shaw, S. (2023). Impact of the interfacial nanolayer on Marangoni convective Darcy-Forchheimer hybrid nanofluid flow over an infinite porous disk with Cattaneo-Christov heat flux. *Thermal Science and Engineering Progress*, *41*, 101854.

[18] Yu, W., and Choi, S. U. S. (2003). The role of interfacial layers in the enhanced thermal conductivity of nanofluids: A renovated maxwell model. *Journal of Nanoparticle Research*, *5*(1), 167–171.

[19] Fan, W., and Zhong, F. (2020). Effects of macro parameters on the thickness of an interfacial nanolayer of Al_2O_3– and TiO_2–water-based nanofluids. *ACS Omega*, *5*(43), 27972–27977.

[20] Xie, H., Fujii, M., and Zhang, X. (2005). Effect of interfacial nanolayer on the effective thermal conductivity of nanoparticle fluid mixture. *International Journal of Heat and Mass Transfer*, *48*(14), 2926–2932.

[21] Alfven, H. (1942). Existence of electromagnetic-hydrodynamic waves. *Nature*, *150*(3805), 405–406.

[22] Rushi Kumar, B., and Sivaraj, R. (2013). Heat and mass transfer in MHD viscoelastic fluid flow over a vertical cone and flat plate with variable viscosity. *International Journal of Heat and Mass Transfer*, *56*(1), 370–379.

[23] Ashwinkumar, G. P., Samrat, S. P., and Sandeep, N. (2021). Convective heat transfer in MHD hybrid nanofluid flow over two different geometries. *International Communications in Heat and Mass Transfer*, *127*, 105563.

[24] Mabood, F., Khan, W. A., and Ismail, A. I. M. (2015). MHD stagnation point flow and heat transfer impinging on stretching sheet with chemical reaction and transpiration. *Chemical Engineering Journal*, *273*, 430–437.

[25] Arshad, M., Hussain, A., Elfasakhany, A., Gouadria, S., Awrejcewicz, J., Pawłowski, W., Elkotb, M.A. and M. Alharbi, F. (2022). Magneto-hydrodynamic flow above exponentially stretchable surface with chemical reaction. *Symmetry*, *14*(8), p.1688.

[26] Akhter, R., Mokaddes Ali, M., and Alim, M. A. (2023). Entropy generation due to hydromagnetic buoyancy-driven hybrid-nanofluid flow in partially heated porous cavity containing heat conductive obstacle. *Alexandria Engineering Journal*, *62*, 17–45.

[27] Sajid, T., Jamshed, W., Safdar, R., Hussain, S.M., Shahzad, F., Bilal, M., Rehman, Z., Rahman, M.M. and Pasha, A.A. (2022). Features and aspects of radioactive flow and slippage velocity on rotating two-phase Prandtl nanofluid with zero mass fluxing and convective constraints. *International Communications in Heat and Mass Transfer*, *136*, p.106180.

[28] Ahmed, S. E., Arafa, A. A. M., and Hussein, S. A. (2022). MHD Ellis nanofluids flow around rotating cone in the presence of motile oxytactic microorganisms. *International Communications in Heat and Mass Transfer*, *134*, 106056.

[29] Abbas, N., Shatanawi, W., Rehman, K. U., and Shatnawi, T. A. M. (2023). Velocity and thermal slips impact on boundary layer flow of micropolar nanofluid over a vertical nonlinear stretched Riga sheet. *Proceedings of the Institution of Mechanical Engineers, Part N: Journal of Nanomaterials, Nanoengineering and Nanosystems*, 23977914231156685.

[30] Arshad, M., Hussain, A., Hassan, A., Shah, S. A. G. A., Elkotab, M. A., Gouadria, S., Alsehli, M. and Galal, A. M. (2022). Heat and mass transfer analysis above an unsteady infinite porous surface with chemical reaction. *Case Studies in Thermal Engineering*, *36*, p.102140.

[31] Haider, F., Hayat, T., and Alsaedi, A. (2021). Flow of hybrid nanofluid through Darcy-Forchheimer porous space with variable characteristics. *Alexandria Engineering Journal*, *60*(3), 3047–3056.

[32] Khan, S. A., Hayat, T., Alsaedi, A., and Alhodaly, M. S. (2022). Thermal analysis for radiative flow of Darcy–Forchheimer nanomaterials subject to entropy generation. *Journal of Computational Design and Engineering*, *9*(5), 1756–1764.

[33] Caucao, S., and Discacciati, M. (2023). A mixed FEM for the coupled Brinkman–Forchheimer/Darcy problem. *Applied Numerical Mathematics*, *190*, 138–154.

[34] Abbas, A., Ashraf, M., Ahmad, H., Ghachem, K., Ullah, Z., Hussanan, A., Labidi, T. and Kolsi, L. (2023). Computational analysis of Darcy-Forchheimer relation, reduced gravity, and external applied magnetic field influence on radiative fluid flow and heat transfer past a sphere: Finite difference method. *Heliyon*, *9*(5).

[35] Maatoug, S., Babu, K. H., Deepthi, V. V. L., Ghachem, K., Raghunath, K., Ganteda, C. and Khan, S. U. (2023). Variable chemical species and thermo-diffusion Darcy–Forchheimer squeezed flow of Jeffrey nanofluid in horizontal channel with viscous dissipation effects. *Journal of the Indian Chemical Society*, *100*(1), p.100831.

[36] Abbas, N., Shatanawi, W., Hasan, F., and Shatnawi, T. (2023). Numerical analysis of Darcy resistant Sutterby nanofluid flow with effect of radiation and chemical reaction over stretching cylinder:

[37] induced magnetic field. *AIMS Mathematics, 8*, 11202–11220.

[38] Ali Pasha, A., Mutiur Rahman, M., Jamshed, W., Ahmed Juhany, K., and Nadaraja, P. S. (2023). Buoyancy driven flow and slippage constraints influences on Casson hybridity nanofluid of Yamada- Ota and Xue type via rotating cone. *Ain Shams Engineering Journal, 14*(4), 101934.

[39] Kiran, B., Fazal, H., Faria, F. and Kashif, A. (2023). Significance of Interfacial Nanolayer and Mixed Convection in Radiative Casson Hybrid Nanofluid Flow by Permeable Rotating Cone. BioNanoScience https://doi.org/10.1007/s12668-023-01191-1.

[40] Li, Y.-M., Khan, M. I., Khan, S. A., Khan, S. U., Shah, Z., and Kumam, P. (2021). An assessment of the mathematical model for estimating of entropy optimized viscous fluid flow towards a rotating cone surface. *Scientific Reports, 11*(1), 10259.